Eur. Phys. J. D **7**, 45–53 (1999)

THE EUROPEAN PHYSICAL JOURNAL D

EDP Sciences

Atomic Rayleigh scattering cross-sections and the associated anomalous dispersion in the X-ray regions

D.V. Rao[1], R. Cesareo[2], and G.E. Gigante[3,a]

[1] Department of Physics, Sir. C.R.R. Autonomous College, C.R.R. Institutions, Eluru-534007, W.G. Dt., A.P., India and The Abdus Salam International Center for Theoretical Physics, 34100 Trieste, Italy
[2] Istituto di Matematica e Fisica, Università di Sassari, Via Vienna 2, 07100 Sassari, Italy
[3] Dipartimento di Fisica, Università di Roma La Sapienza, P.le A. Moro 2, 00185 Roma, Italy

Received: 27 January 1998 / Received in final form: 4 January 1999

Abstract. Elastic scattering cross-sections for Pd, Ag, Cd, In, Sn, Sb, Pt, Au and Pb are measured at an angle of 90° in the X-ray region $5.41 \leq E \leq 8.04$ keV. These energies fall between the high-energy side of the L- and M-shell absorption edges of the atoms considered. The present atomic region is significant for solid X-rays to assess the contribution of resonance and solid-state environmental effects. Also it is the anomalous scattering region for many of the atoms of the periodic table. Experimental results are compared with theoretical calculations based on form factor formalisms including the anomalous corrections and available recent S-matrix values. Based on the experimental evidence, the present results indicate the influence of solid-state environmental effects, the importance of anomalous corrections nearer to absorption edges, the correctness of revised high-energy limit values, the superiority of S-matrix predictions over form factor values on measured elastic scattering cross-sections in the X-ray regime and also show the resonance behavior around K, L and M absorption edges.

PACS. 78.70.-g Interactions of particles and radiation with matter – 78.70.Ck X-ray scattering – 61.10.Eq X-ray scattering (including small-angle scattering)

1 Introduction

Elastic scattering of low-energy X-ray photons from neutral atoms by bound atomic electrons is usually called Rayleigh scattering. It arises from a collision between the photon and the atom as a whole, since the effective photon mass is completely negligible compared with that of the atom, the elastically scattered photon carries away all its initial energy. Anomalies occur in the vicinity of absorption edges and the cross-section is in general small [1]. It gives us information about the inner structure of the atoms and macromolecules [2], in medical diagnostics and imaging [3]. There are numerous approaches for calculating the Rayleigh scattering cross-section for atoms. The form factor approximation to the Rayleigh scattering of photons by atoms is the simplest and most widely used approach, which predicts problems associated with absorption edges. The atomic form factor for anomalous dispersion can be written as

$$f(q) = f_0(q) + f' + f'' \,. \tag{1}$$

In the above expression $f_0(q)$ is the normal atomic form factor computed at the energy-angle combination. The quantities f' and f'' are the real and imaginary parts of the correction to $f_0(q)$ arising from anomalous dispersion.

The calculation of the dispersion term is straightforward in case of forward scattering ($\theta = 0$). The imaginary part of the dispersion correction is proportional to the total photoelectric cross-section $\sigma_{\rm ph}$ at the photon energy $\hbar\omega$. Then f'' is given by the optical theorem

$$f'' = \frac{1}{r_0}\frac{\hbar\omega}{4\pi\,\hbar c}\sigma_{\rm ph}(\hbar\omega)\,. \tag{2}$$

The real part of the dispersion correction in the forward direction, where $f_0 \cong Z$, is

$$f' = f'(\infty) - \frac{2}{\pi}\mathrm{P}\int_0^\infty \frac{\omega' f''(\omega')}{\omega^2 - \omega'^2}\mathrm{d}\omega'\,, \tag{3}$$

here $\hbar\omega$ is the X-ray energy, $\sigma_{\rm ph}$ $(\hbar\omega)$ is the total photoelectric cross-section and P represents the principal value. Extensive and accurate values of f' and f'' are required for the normalisation of the experimental data [4,5] and also useful for various applications [5].

Extensive theoretical tabulations based on non-relativistic form factors [7], relativistic form factors [8], relativistic modified form factors [9] and relativistic numerical calculations based on the multipole expansion of the second-order S-matrix approach [10] are available in the

[a] e-mail: g.gigante@caspur.it

literature. Elastic photon scattering is assessed with the aid of the relativistic numerical calculation of Rayleigh scattering using S-matrix theory [11]. Recently, the validity of the form factor, the modified form factor and anomalous scattering approximations in elastic scattering calculations have been studied extensively in the K absorption edge region [12]. In the vicinity of an atom absorption edge there can be significant corrections to the atomic form factor. The available calculated values describe the free atom and deviations for a solid have to be expected. However, very few experimental measurements are available in the low-energy X-ray region [13–17]. The deviations are observed in earlier investigations [18] on the high-energy side of the absorption edges. To explain the difference of the electronic structure of the solid in comparison to the free atom as a base for theoretical estimations, measurements around the edges were performed with Pd, Ag, Cd, In, S, Sb, Pt, Au and Pb in the energy region $5.41 \leq E \leq 8.04$ keV.

2 Theoretical methods

A comprehensive knowledge of the form factor, *i.e.*, including real and imaginary parts of the anomalous dispersion correction is worthwhile since a knowledge of one electron charge distribution provides a detailed description of the electronic structure of the system.

The atomic form factor $f(q)$ for a spherically symmetric atom can be expressed in the following way [19]:

$$f(q) = 4\pi \int_0^\infty \rho(r) \frac{\sin(qr)}{(qr)} r^2 \mathrm{d}r \,. \tag{4}$$

The scattering cross-section can be obtained by multiplying the Thompson cross-section by the square of the form factor

$$\mathrm{d}\sigma/\mathrm{d}\Omega = (\mathrm{d}\sigma/\mathrm{d}\Omega)_\mathrm{T} |f(q)|^2 \,, \tag{5}$$

where q is the magnitude of the momentum transfer between the initial photon and an electron.

Franz [20] suggested an electron binding correction to the form factor and the resulting form factor is represented by $g_i(q)$. The modified form factor for a given electron is given by

$$g_i(q) = 4\pi \int_0^\infty \rho(r) \frac{\sin(qr)}{(qr)} \frac{mc^2}{E_i - V(r)} r^2 \mathrm{d}r \,, \tag{6}$$

where E_i is the total energy of the i-th electron ($E = mc^2 - \varepsilon_k, \varepsilon_k$ is the electron binding energy, $V(r)$ is the atomic potential, and $\rho(r)$ is the charge distribution associated with the i-th electron. It is to be noted in this connection that unlike $f(q)$, due to the presence of the term ε_k, $g_i(q)$ cannot be calculated directly from the total atom charge distribution; instead, contributions from all subshell electrons should be taken into account separately. The corresponding cross-sections for unpolarised photons in modified form factor is given by

$$\mathrm{d}\sigma/\mathrm{d}\Omega = \frac{r_0^2}{2}(1 + \cos^2\theta)|g(q)|^2 \,, \tag{7}$$

Table 1. High-energy limit values for photon scattering in the atomic region $46 \leq Z \leq 82$.

Atom	$f(0)$	$g(0)$	$f'_{\mathrm{CL}}(\infty)$	$f'_{\mathrm{SM}}(\infty)$	$\delta f'$	$\delta g'$
Pd	46	45.749	−0.447	−0.251	0.196	0.447
Ag	47	46.736	−0.471	−0.264	0.207	0.471
Cd	48	47.723	−0.496	−0.277	0.219	0.496
In	49	48.709	−0.521	−0.291	0.230	0.521
Sn	50	49.695	−0.547	−0.305	0.242	0.547
Sb	51	50.680	−0.575	−0.320	0.255	0.575
Pt	78	77.126	−1.636	−0.874	0.762	1.636
Au	79	78.099	−1.689	−0.901	0.788	1.689
Pb	82	81.104	−1.856	−0.986	0.814	1.856

replacing $|f(q)|^2$ by $|g(q)|^2$ in equation (2).

The form factor approximation has also been derived in non-relativistic and relativistic quantum mechanics. The form factor for elastic scattering is valid when the electron binding energy is small compared with the photon energy. In non-relativistic theory Rayleigh scattering arises through the photon-electron interaction, Hamiltonian terms $e^2\mathbf{A}\cdot\mathbf{A}/2mc$ and $(-e\mathbf{P}\cdot\mathbf{A}/mc)$, where $\mathbf{A}$ is the vector potential of the radiation and $\mathbf{P}$ is the electron momentum operator. The A^2-dependent term alone leads to the form factor description of atomic Rayleigh scattering cross-section. The $P\cdot A$ interaction term alone leads to the introduction of explicitly energy-dependent real and imaginary anomalous scattering factors of f' and f'' or g' and g'', in the two schemes respectively. Accordingly in equations (2) and (4) for atomic Rayleigh scattering cross-section, $|f(q)|^2$ and $|g(q)|^2$ will be replaced by $|f(q) + f'| + f''^2$ and $|g(q) + g'| + g''^2$. The contribution of the photoeffect to the optical theorem depends on the photon energy considered, bound-bound transitions, and pair production at high energies. The dominant part of the anomalous scattering factors f'' and g'' in the forward direction is proportional to the photoeffect cross-section at the same energy. The optical theorem is connected to the evaluation of the imaginary part f''. A dispersion relation connecting the real and the imaginary parts of the Rayleigh amplitudes is then used to calculate the real part of the anomalous scattering functions.

2.1 Anomalous scattering factors

The real quantities f', f'' and g', g'' are called the anomalous scattering factors. They give a deviation of the forward-scattering amplitude from the form factor and the modified form factor.

Cromer and Liberman [21] used the dipole approximation to compute the high-energy limit f' as

$$f'_{\mathrm{CL}} = \frac{5}{3}\frac{E_{\mathrm{tot}}}{mc^2} \,, \tag{8}$$

where E_{tot} is the total ground-state energy of the atom. This use of dipole approximation to compute the high-

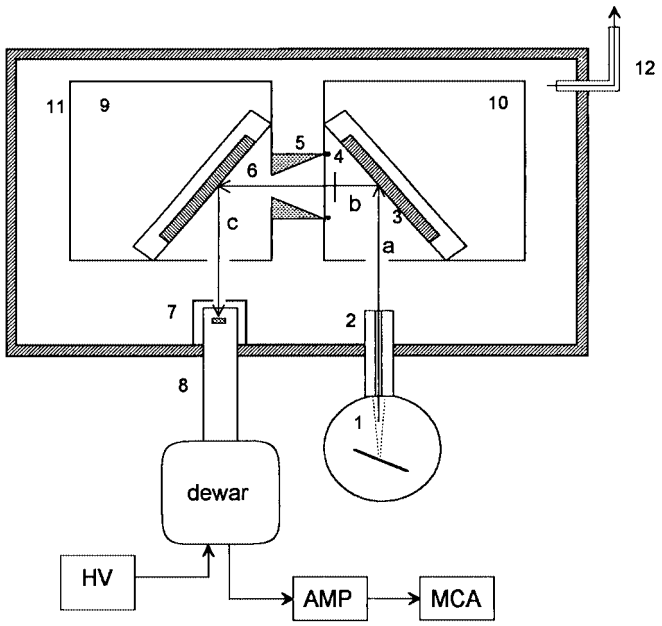

Fig. 1. Schematic setup of the apparatus employed for the present measurements. 1 = X-ray tube, 2 = collimator, 3 = secondary target, 4 = filter, 5 = conical collimator, 6 = sample, 7 = detector collimator, 8 = Si (Li) detector, 9 and 10 are thick brass holders, 11 = vacuum pump, 12 = vacuum chamber.

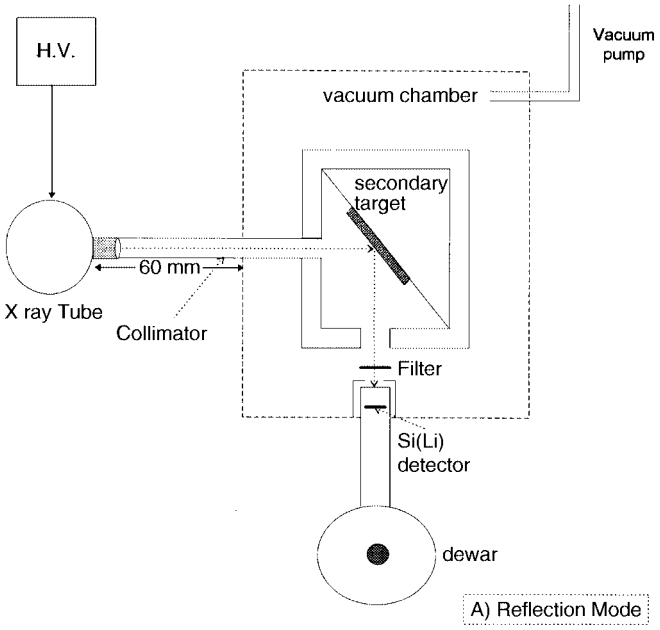

Fig. 2. Experimental arrangement used to estimate the flux emitted from the secondary target.

energy limit results in an error that affect their f' values at all energies.

The high-energy limit of the S-matrix approach is very accurately predicted by the relativistic modified form factor

$$f'_{\mathrm{CL}}(\infty) = -f(0) + g(0)\,. \tag{9}$$

The f' values of Cromer and Liberman are not entirely correct due to the incorrect treatment of the high-energy limit. Kissel and Pratt [22] defined the needed energy-independent correction term as

$$f'_{\mathrm{CCL}}(\infty)=f'_{\mathrm{CL}}(\omega)+\delta f'',\ \text{where}\ \delta f'=-f'_{\mathrm{CL}}(\infty)+f'_{\mathrm{SM}}(\infty). \tag{10}$$

In using Cromer and Libermans tables [23] one should include this factor. Similarly an anomalous scattering factor for use with the relativistic modified form factor could be defined as

$$g'_{\mathrm{CCL}}(\omega) = f'_{\mathrm{CCL}}(\omega) + \delta g',\ \text{where}\ \delta g' = -f'_{\mathrm{CL}}(\infty)\,. \tag{11}$$

The high-energy limit values and the anomalous scattering factors used in the present work are presented in Tables 1 and 2.

3 Experimental details

An X-ray tube with tungsten anode and a secondary target arrangement has been used for the present measurements. The experimental arrangement and the geometry used are shown in Figure 1. Figure 2 shows the experimental arrangement used to estimate the flux emitted by the secondary target. The X-ray tube maximum voltage and current are 55 kV and 30 mA. The secondary targets Cr, Fe, Co, Ni and Cu were pure metals and provided the 5.41, 6.40, 6.93, 7.47 and 8.04 keV X-ray photons. Spectroscopically pure samples of Pd, Ag, Cd, In, Sb, Sn, Pt, Au and Pb thickness ranging from 0.35 to 2.40 g/cm^2 have been used. The scattered spectra from various samples were detected with a Si(Li) detector (active diameter 10 mm eV (FWHM) of 155 eV at 5.96 keV) coupled to a 1024 computerised multichannel analyser through a spectroscopy fine tuning research amplifier. The built-in computer aided with data storage, background subtraction, and determination of the net area of the X-ray line. Figures 3 and 4 show the scattered spectra of Cr and Co $K\alpha$ photons from Pd, Cd, In and Sb. Figures 5 and 6 show the scattered spectra of Co $K\alpha$ photons from Au and Pb. Figure 7 shows the scattered spectra of Mn $K\alpha$ photons from Pt. The peaks are well resolved and the degree of monochromaticity is reasonable. To reduce the statistical error in the measurements, two or more samples of different thickness were used. Two spectra were recorded for the time intervals ranging from 1000 to 2000 s.

The aim of obtaining accurate and precise results suggests the choice of a simple geometrical arrangement, *i.e.*, reflection geometry with both the source and the detector equipped with collimators., *i.e.*, the axes of the incident and observed beams made the same angle with the normal to the scattering sample. Moreover, the distances between the source and scatterer and between the scatterer and detector were equal in practice and very large in comparison to the dimensions of the scattering surface seen by the detector, hence this surface practically belonged to a

Table 2. Anomalous scattering factors in the energy region $5.41 \leq E \leq 8.04$ keV for Pd, Ag, Cd, In, Sn, Sb, Pt, Au and Pb. CL indicates the anomalous scattering factors of Cromer and Liberman [21,23]. CCL indicates CL data plus high-energy corrected anomalous scattering factors.

5.41 keV					6.40 keV				
Z	$f''_{\rm CL}$	$f'_{\rm CL}$	$f'_{\rm CCL}$	$g'_{\rm CCL}$	Z	$f''_{\rm CL}$	$f'_{\rm CL}$	$f'_{\rm CCL}$	$g'_{\rm CCL}$
Pd	7.594	−0.639	−0.443	−0.192	Pd	5.773	−0.157	0.039	0.290
Ag	8.235	−0.924	−0.717	−0.453	Ag	6.271	−0.259	−0.052	0.212
Cd	8.912	−1.303	−1.084	−0.807	Cd	6.800	−0.416	−0.197	0.080
In	9.627	−1.788	−1.550	−1.259	In	7.356	−0.626	−0.396	−0.105
Sn	10.380	−2.401	−2.159	−1.854	Sn	7.943	−0.888	−0.646	−0.341
Pt	12.787	−4.584	−3.822	−2.948	Pt	9.895	−4.535	−3.773	−2.899
Au	13.451	−4.668	−3.880	−2.979	Au	10.418	−4.510	−3.722	−2.821
Pb	15.595	−5.610	−4.347	−3.305	Pb	12.108	−4.596	−3.782	−2.740
6.93 keV					7.47 keV				
Z	$f''_{\rm CL}$	$f'_{\rm CL}$	$f'_{\rm CCL}$	$g'_{\rm CCL}$	Z	$f''_{\rm CL}$	$f'_{\rm CL}$	$f'_{\rm CCL}$	$g'_{\rm CCL}$
Pd	5.06	−0.061	0.136	0.387	Pd	4.510	−0.060	0.136	0.387
Ag	5.50	−0.142	0.067	0.331	Ag	4.906	−0.101	0.106	0.320
Cd	5.96	−0.260	0.041	0.236	Cd	5.322	−0.169	0.050	0.327
In	6.46	−0.373	−0.140	0.151	In	5.774	−0.190	0.040	0.331
Sn	6.98	−0.544	−0.298	0.007	Sn	6.240	−0.372	−0.130	0.171
Sb	7.52	−0.752	−0.495	−0.175	Sb	6.727	−0.534	−0.279	0.041
Pt	8.74	−4.673	−3.908	−3.304	Pt	7.859	−4.944	−4.182	−3.308
Au	9.21	−4.584	−3.792	−2.891	Au	8.281	−4.831	−4.043	−3.142
Pb	10.71	−4.061	−3.786	−2.744	Pb	9.844	−4.706	−3.892	−2.850
8.04 keV									
Z	$f''_{\rm CL}$	$f'_{\rm CL}$	$f'_{\rm CCL}$	$g'_{\rm CCL}$					
Pd	3.934	−0.059	0.137	0.388					
Ag	4.282	−0.060	0.147	0.411					
Cd	4.653	−0.079	0.140	0.417					
In	5.045	−0.126	0.104	0.395					
Sn	5.459	−0.194	0.048	0.353					
Sb	5.894	−0.287	−0.032	0.288					
Pt	6.925	−5.233	−4.471	−3.597					
Au	7.297	−5.096	−4.308	−3.407					
Pb	8.930	−4.818	−4.004	−2.962					
$f''_{\rm CL} = f''_{\rm CCL}$; $f'_{\rm CCL} = f'_{\rm CL} + \delta f'$; $g'_{\rm CCL} = g'_{\rm CL} + \delta g'$									

constant scattering-angle surface [24,25]. A new method is developed to estimate the degree of monochromaticity, efficiency and geometrical effects of the measuring system, solid angle correction and some considerations on bremsstrahlung-induced fluorescent radiation. The need of these parameters and their use in secondary target arrangements are thoroughly discussed and reported elsewhere [26].

The detector has been calibrated using X-ray sources, the energy and FWHM have been calculated using the following relations:

$$E = a_0^* \text{channel} + a_1^* \text{channel}^2 + a_2^* \text{channel}^3 \quad (12)$$

$$\text{FWHM} = b_0 + b_1 E + b_2 E^2 \,, \quad (13)$$

where a_0, a_1 and a_2 are the fitted coefficients for the energy calibration and b_0, b_1 and b_2 are the fitted coefficients for the full width at half maximum, E is the energy of the emitted elastic peak. The estimation of background and the data analysis are similar to our earlier investigations [27]. The elastically scattered $K\alpha$ radiation was corrected for the background in order to calculate the net area under the peak. Figure 7 shows the Gaussian fit of the scattered spectra of 5.41 keV Mn $K\alpha$ photons from Pt. In the fitting procedure, the peak shape and background subtraction are described by a mathematical function with the energy as a variable and a number of parameters that can be varied freely. The function is then fitted to some preselected interval of the spectra by varying the parameters. The function in the present study can be written as follows:

$$f(x) = Y_0 + \sqrt{\frac{2}{\pi}} \frac{A}{W} e^{-2(X - X_{\rm c})/X_{\rm c}} \,, \quad (14)$$

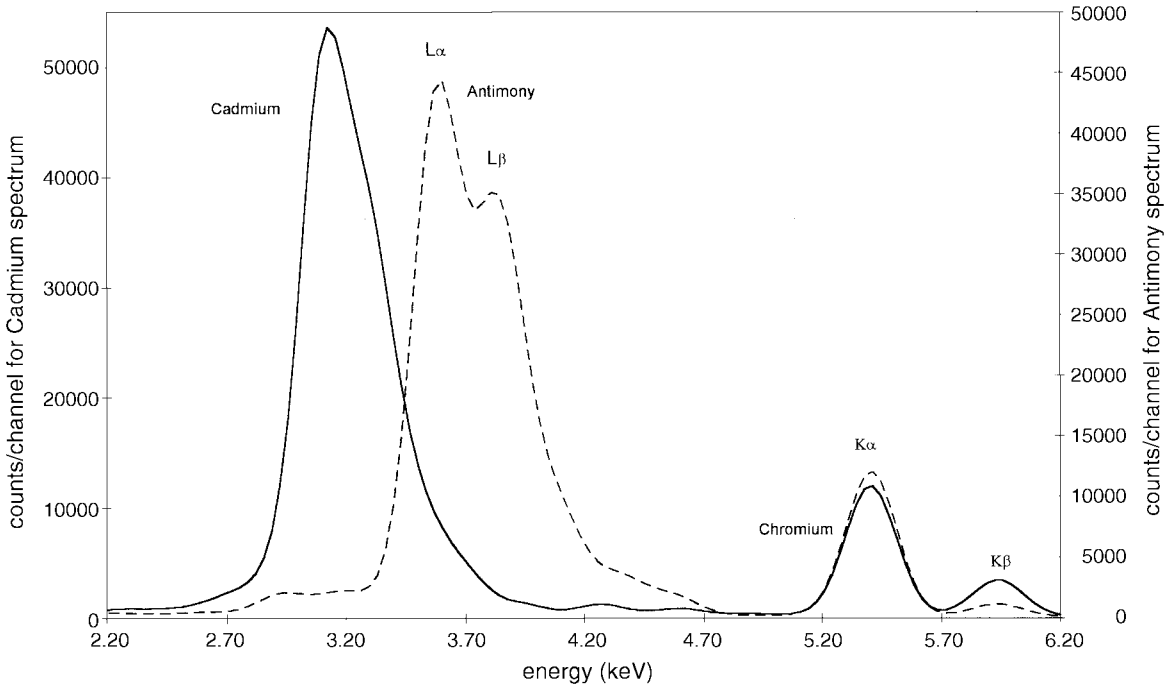

Fig. 3. Scattered spectra of 5.41 keV (Cr $K\alpha + K\beta$) photons from Cd and Sb including total L X-ray peaks due to fluorescence.

where Y_0 is the background, X = energy, A = peak area, X_c is the centroid of the elastically scattered peak with in the interval and $W = 0.75\,\mathrm{FWHM}$. To overcome the experimental error arises due to this convolution procedure the statistical error was always maintained less than 1%.

3.1 Experimental procedure

The characteristic $K\alpha$ X-ray line energies of the secondary targets are elastically scattered by the sample into the detector. The differential elastic scattering cross-sections were evaluated using the following relation:

$$(\mathrm{d}\sigma/\mathrm{d}\Omega)_{\mathrm{ela}} = N_{\mathrm{ela}}[I_0(E)t_{\mathrm{ela}}(\rho D)\varepsilon_{\mathrm{ela}}]^{-1}\,, \qquad (15)$$

where N_{ela} is the area under the elastically scattered $K\alpha$ radiation from the sample, $I_0(E)$ is the incident beam intensity at the target, ρD is the sample mass per unit area in $\mathrm{gm/cm^2}$, $\varepsilon_{\mathrm{ela}}$ is the detector efficiency for the elastically scattered radiation and t_{ela} is the absorption correction term [28]. The method of evaluation of incident beam intensity and absorption correction terms were thoroughly discussed in earlier investigations [29].

4 Results and discussion

Experimental elastic scattering cross-sections and theoretical calculations are presented in Table 3. Theoretical values obtained through various approximations are very close to one another and experimental results differ by 12%. It is interesting to note that a relatively good-theory experiment is reached. More attention has been focused on calculation of scattering in the range $5.41 \leq E \leq 8.04$ keV. It is the anomalous scattering region for many of the atoms of the periodic table. These energies fall between the L- and M-shell photoeffect thresholds of the atoms considered in the present study. Experimental results are compared with the theoretical calculations based on non-relativistic form factors, relativistic form factors, relativistic modified form factors and relativistic numerical calculation based on the multipole expansion of the second-order S-matrix approach. Experimental scattering cross-sections are compared with theoretical calculations by adding the anomalous scattering factors (NRF+CL, RFF+CL, RMF+CL) and high-energy limit values (NRF+CCL, RFF+CCL, RMF+CCL).

NRF, RFF and RMF were high-energy approximations at low momentum transfer region and considerable deviations for photon energies above, below and nearer to the photoeffect thresholds and for heavy elements at large momentum transfers. With the inclusion of electron binding effects into the form factor, the modified form factor produces better high-energy limits for heavy elements and gives the correct relativistic high-energy limit for forward scattering. However, good results can be obtained with the inclusion of anomalous scattering factors to NRF, RFF and RMF to correct these values for forward scattering. Relativistic calculations based on the multipole expansion of the second-order matrix are available in the literature for few elements for comparison of the present measurements. With the inclusion of all the significant multipoles and partial waves in the radiation interaction with the scattering electron in the atomic potential, the S-matrix method gives excellent results at low and high momentum transfer regions.

Table 3. Comparison of experimental elastic-scattering cross-sections (b/atom) with theoretical calculations in the atomic region $46 \leq Z \leq 82$ at 5.41, 6.40, 6.93, 7.47 and 8.04 keV incident photon energies. NRF = Non-relativistic form factor, RFF = Relativistic form factor, RMF = Relativistic modified form factor. CL = Anomalous scattering factors of Cromer and Liberman [21,23], CCL = Anomalous scattering factors of Cromer and Liberman corrected for the high-energy limit. SM = S-matrix values, Exp = Experimental values.

5.41 keV

Z	NRF	NRF + CL	NRF +CCL	RFF	RFF + CL	RFF +CCL	RMF	RMF + CL	RMF +CCL		EXP
Pd	38.2	38.9	39.4	38.3	39.0	39.5	37.6	38.3	39.4		40.8 ± 4.0
Ag	40.4	40.8	41.3	40.8	41.2	41.7	39.8	40.2	41.3		42.6 ± 4.2
Cd	42.5	42.3	42.9	43.9	42.8	43.4	42.2	41.9	43.1		43.9 ± 4.3
In	44.7	43.7	44.3	44.6	43.6	44.3	44.1	43.2	44.5		44.2 ± 4.4
Sn	46.7	44.6	45.2	47.2	44.9	45.6	45.8	43.8	45.2		46.3 ± 4.5
Sb	48.5	45.0	45.6	48.7	45.2	45.8	47.7	44.3	45.7		46.7 ± 4.6
Pt	132.0	118.0	122.0	134.0	120.0	123.0	129.0	116.0	123.0	123	124.0 ± 12.0
Au	136.0	122.0	126.0	137.0	123.0	126.0	133.0	119.0	127.0	127	129.0 ± 12.2
Pb	147.0	137.0	136.0	149.0	134.0	138.0	143.0	129.0	137.0	138	140.0 ± 14.4

6.40 keV

Z	NRF	NRF + CL	NRF +CCL	RFF	RFF + CL	RFF +CCL	RMF	RMF + CL	RMF +CCL		EXP
Pd	31.8	32.9	33.30	32.0	33.0	33.5	31.6	32.5	33.6		34.4 ± 3.0
Ag	33.6	34.6	35.0	33.9	34.9	35.3	33.3	34.2	35.3		36.1 ± 3.2
Cd	35.5	37.0	36.9	35.8	36.6	37.1	35.0	35.9	37.1		38.5 ± 3.4
In	37.5	38.1	38.7	37.7	38.4	38.9	36.9	37.6	38.8		40.2 ± 3.8
Sn	39.4	39.7	40.3	39.6	39.9	40.5	38.8	39.1	40.4		41.7 ± 4.0
Sb	41.2	41.0	41.7	41.5	41.3	42.3	40.5	40.4	41.8		43.8 ± 4.2
Pt	115.0	99.0	103.0	116.0	102.0	105.0	112.0	97.9	104.0	105	106.0 ± 9.8
Au	118.0	103.0	107.0	119.0	105.0	108.0	115.0	101.0	108.0	108	109.0 ± 10.0
Pb	128.0	114.0	117.0	130.0	115.0	119.0	125.0	111.0	119.0	119	120.0 ± 10.8

6.93 keV

Z	NRF	NRF + CL	NRF +CCL	RFF	RFF + CL	RFF +CCL	RMF	RMF + CL	RMF +CCL		EXP
Pd	29.0	29.9	30.3	29.3	30.2	30.6	28.8	27.7	30.7		31.7 ± 3.0
Ag	30.6	31.5	32.0	31.3	31.8	32.2	30.4	31.3	32.3		33.4 ± 3.1
Cd	32.3	33.2	33.7	32.6	33.5	34.0	32.0	32.8	33.9		34.6 ± 3.4
In	34.2	35.0	35.5	34.4	35.2	35.8	33.7	34.5	35.7		36.7 ± 3.6
Sn	36.0	36.6	37.2	36.3	36.9	37.5	35.0	35.7	36.9		38.1 ± 3.6
Sb	37.8	38.2	38.8	38.0	38.5	39.1	37.2	37.6	39.0		40.2 ± 3.8
Pt	106.0	91.1	94.0	108.0	92.6	95.6	105.0	89.4	95.6	96	97.1 ± 9.2
Au	109.0	94.3	97.3	110.0	95.9	98.9	108.0	92.6	99.0	99	103.0 ± 9.6
Pb	119.0	104.0	108.0	121.0	106.0	109.0	116.0	102.0	109.0	110	114.0 ± 9.8

7.47 keV

Z	NRF	NRF + CL	NRF +CCL	RFF	RFF + CL	RFF +CCL	RMF	RMF + CL	RMF +CCL		EXP
Pd	26.5	27.2	27.6	26.8	27.5	27.9	26.4	27.1	28.0		28.6 ± 2.4
Ag	27.9	28.7	29.1	28.3	29.1	29.5	27.8	28.5	29.5		30.2 ± 3.0
Cd	29.5	30.3	30.7	29.8	30.6	31.0	29.3	30.3	31.1		31.9 ± 3.1
In	31.1	32.1	32.6	31.4	32.1	32.9	30.8	31.7	32.9		34.2 ± 3.3
Sn	32.8	33.5	34.1	33.1	33.8	34.4	32.4	33.1	34.3		36.0 ± 3.6
Sb	34.5	35.1	35.7	34.8	35.4	36.0	34.0	34.6	35.9		37.2 ± 3.7
Pt	97.8	82.6	85.4	97.1	84.2	90.2	97.1	81.1	87.0		88.3 ± 9.5
Au	101.0	85.6	88.5	102.0	87.3	93.6	99.7	84.1	90.3	90	91.9 ± 9.8
Pb	111.0	95.5	98.7	112.0	97.0	100.0	108.0	93.3	100.0	101	104.0 ± 9.9

8.04 keV

Z	NRF	NRF + CL	NRF +CCL	RFF	RFF + CL	RFF +CCL	RMF	RMF + CL	RMF +CCL		EXP
Pd	24.3	24.8	25.1	24.5	25.0	25.3	24.7	25.2	26.0		27.4 ± 3.2
Ag	25.5	26.1	26.5	25.7	26.3	26.7	25.3	25.9	26.8		28.1 ± 3.4
Cd	26.9	27.6	28.0	27.1	27.8	28.2	26.6	27.3	28.3		30.3 ± 3.6
In	28.4	29.1	29.6	28.6	29.3	29.8	28.0	28.7	29.8		31.9 ± 3.8
Sn	29.9	30.7	31.2	30.1	30.9	31.4	29.5	30.2	31.4		33.6 ± 4.0
Sb	31.6	32.3	32.9	31.6	32.4	33.0	31.0	32.4	33.0		35.2 ± 4.2
Pt	91.6	74.7	77.3	93.1	76.0	78.6	89.8	73.0	78.6	79	80.2 ± 12.0
Au	94.0	77.5	80.2	95.6	78.9	81.6	92.2	75.8	81.7	82	82.2 ± 12.4
Pb	103.0	87.1	90.1	104.0	88.1	91.2	100.0	84.9	91.8	92	93.2 ± 12.6

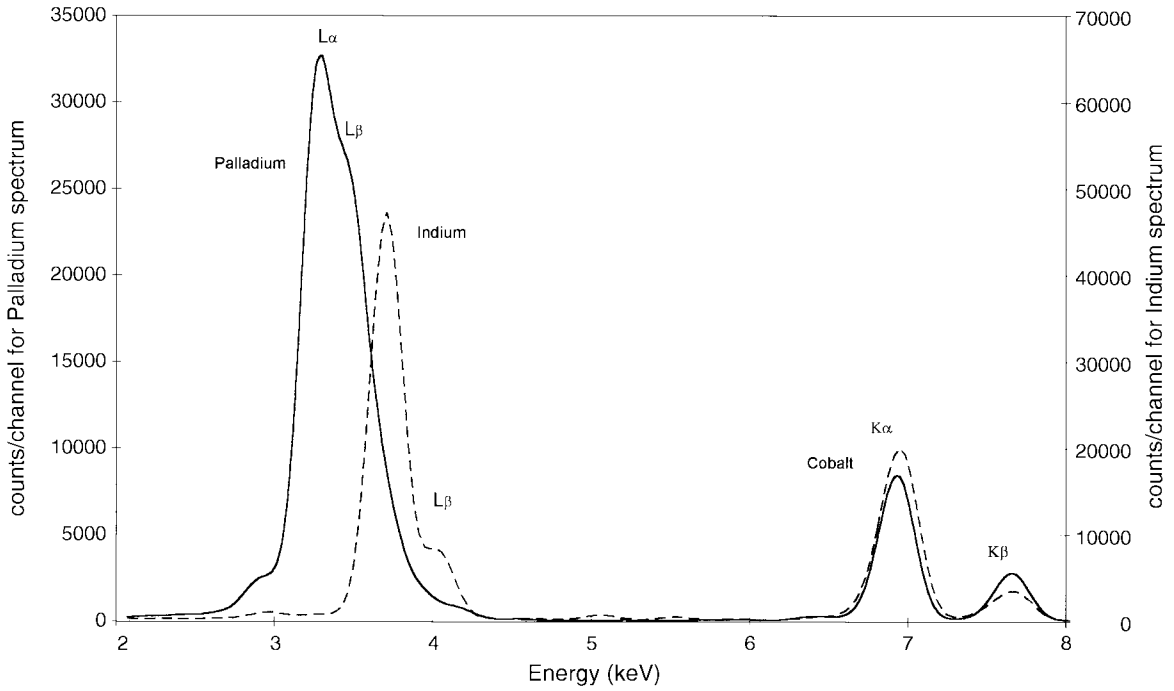

Fig. 4. Scattered spectra of 6.93 keV (Co $K\alpha + K\beta$) photons from Pd and In including the total L X-ray peaks due to fluorescence.

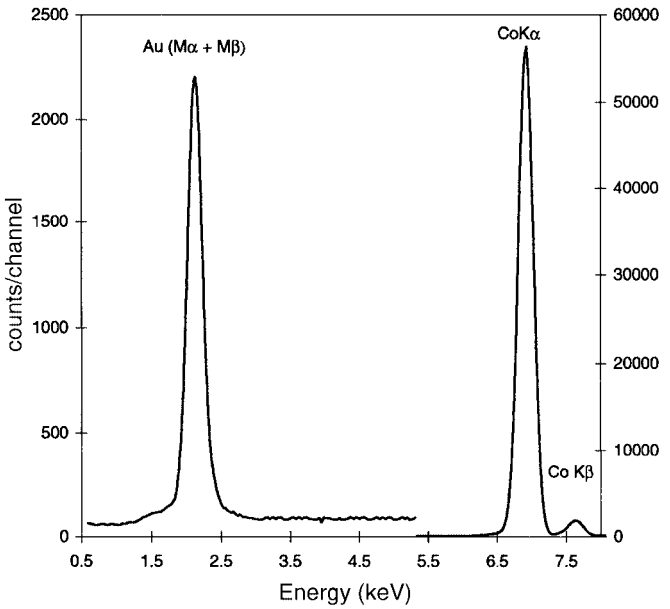

Fig. 5. Scattered spectra of 6.93 keV (Co $K\alpha + K\beta$) photons from Au including the total M X-ray peak due to fluorescence.

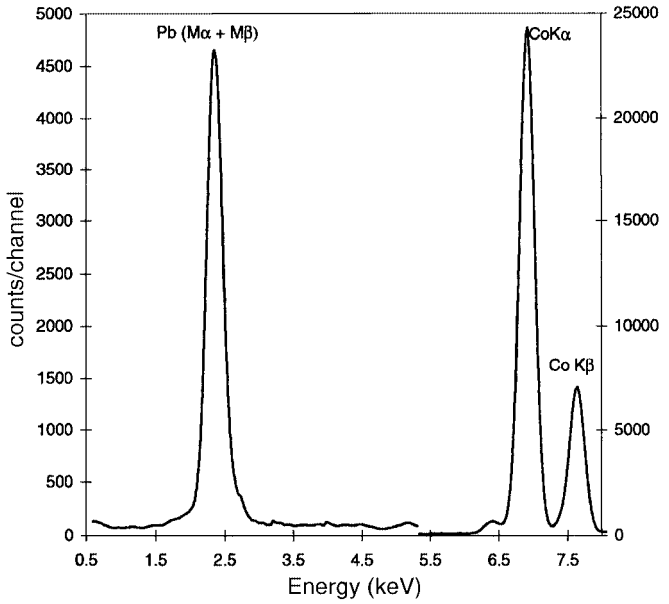

Fig. 6. Scattered spectra of 6.93 keV (Co $K\alpha + K\beta$) photons from Pb including the total M X-ray peak due to fluorescence.

The cross-sections calculated with a combination of NRF+CCL, RFF+CCL and RMF+CCL are larger than NRF+CL, RFF+CL and RMF+CL values in the atomic region $46 \leq Z \leq 51$ at all the energies and smaller in the atomic region $78 \leq Z \leq 82$. The contribution of real and imaginary parts is considerably high for Pt, Au and Pb at these energies.

At 5.41 keV in the atomic region $46 \leq Z \leq 51$, the ratios $f^2(q)/|f(q)+f'|+f''^2$ and $g^2(q)/|g(q)+g'|+g''$ vary from 0.981 to 1.078 and from 1.15 to 1.108 in the atomic region $78 \leq Z \leq 82$. The ratios f''^2/f' and g''^2/g' change from 0.06 to 0.1 in the atomic region $46 \leq Z \leq 51$ and from 0.05 to 0.07 in the atomic region $78 \leq Z \leq 82$. The ratios $f''/f(q)$ and $g''/g(q)$ change from 0.021 to -0.091 in the atomic region $46 \leq Z \leq 51$ and from -0.079 to

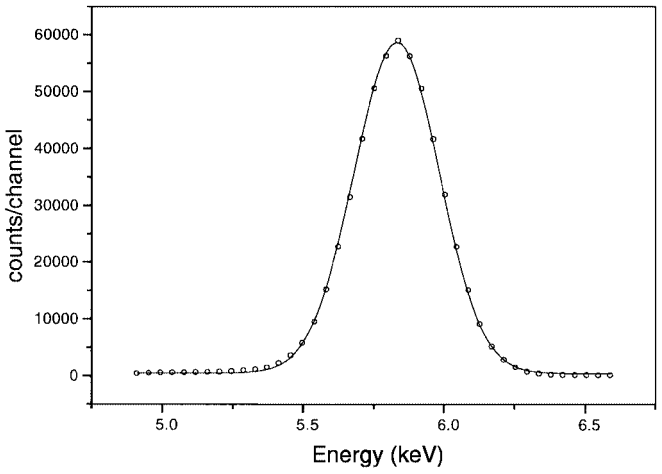

Fig. 7. Scattered spectra of 5.41 keV (Mn $K\alpha$) photons from Pt (∘ indicates experimental points, — indicates the Gaussian fit).

-0.086 in the region $78 \leq Z \leq 82$. In this region the maximum anomalous dispersion occurs.

At 8.04 keV the ratios f''/f^2 and g''/g^2 vary from 0.03 to 0.04 in the atomic region $46 \leq Z \leq 51$ and from 0.05 to 0.03 in the atomic region $78 \leq Z \leq 82$. The ratios $f'/f(q)$ and $g'/g(q)$ vary from -0.002 to -0.01 in the atomic region $46 \leq Z \leq 51$ and from -0.108 to -0.096 in the region $78 \leq Z \leq 82$. The relative contribution of f'/f and f''/f is estimated in order to assess the importance of the above ratios on ordered structures. At 6.93 keV the relative contribution of f'/f and g'/g varies from 0.002 to 0.024 in the atomic region $46 \leq Z \leq 51$ and from 0.098 to 0.088 in the atomic region $78 \leq Z \leq 82$. The ratios of f''^2/f and g''^2/g vary from 0.035 to 0.059 in the atomic region $46 \leq Z \leq 51$ and from 0.0278 to 0.0376 in the atomic region $78 \leq Z \leq 82$. The above type of analysis at other incident photon energies indicates the importance of anomalous dispersion correction terms.

The percentage of deviation of the theoretical calculations with experimental cross-sections shows positive and negative deviation and in particular on the high-energy side of the absorption edges. With the inclusion of the anomalous scattering factors the deviation has been reduced enormously. More experimental studies are needed to explore the new possibilities of deviation of the elastic scattering cross-section from the ordered structures.

We have estimated the average error (χ) using the experimental results and the recent theoretical results based on the S-matrix approach for Pt, Au and Pb in the energy region $5.41 \leq E \leq 8.04$ keV:

$$\chi = (\sigma_{\rm exp} - \sigma_{\rm SM})/\Delta\,, \tag{16}$$

where Δ is the experimental error in the last column of Table 3. The average error is below 1% for Pt, Au and Pb with values based on the S-matrix approach. The same trend has been observed on theories based on form factor formalisms with the inclusion of anomalous values. In all the cases $\chi^2/n < 1$ and the uncertainty estimates are correct.

Fairly good correspondence is observed between the experimental results and the theoretical calculations corrected for anomalous scattering (NRF+CL, RFF+CL and RMF+CL) compared to uncorrected theoretical calculations (NRF<RFF and RMF). Experimental results are in excellent agreement with the theoretical calculations corrected for the high-energy limit (NRF+CCL, RFF+CCL and RMF+CCL) and S-matrix values compared to theoretical calculations corrected using the anomalous scattering factors (NRF+CL, RFF+CL and RMF+CL) differ by less than 5%. However, the present results indicate the influence of solid-state environmental effects on measured cross-sections, the importance of anomalous corrections near to absorption edges, the superiority of S-matrix predictions over form factor formalisms, the correctness of high-energy limit values and show resonance behaviour around absorption edges.

5 Conclusions

The present experimental results are useful taking into account that the available calculated values describe the free atom and the deviations for a solid have to be expected. The deviations are observed on the high-energy side of the absorption edges. This is due to the difference of the electronic structure of the solid in comparison to the free atom as a base for theoretical estimations. Also the present results indicate the importance of the high-energy limit values in the absence of the very recent theoretical S-matrix values. Further experimental work is in progress at still lower photon energies which covers most of the medium- and high-Z region.

We are very grateful to Prof. Dr. G. Furlan for providing the financial assistance and also the Istituto di Matematica e Fisica, Università di Sassari, Italy for allowing us to carry out the experimental work. One of us (DVR) undertook this work with the support of the ICTP programme for training and research in Italian laboratories, Trieste, Italy and University Grants Commission, New Delhi, India.

References

1. A.H. Compton, S.K. Allison, *X-rays in Theory and Experiment*, 2nd edition (Van Nostrand, New York, 1935).
2. J. Karle, Phys.Today, **42**, N° 6, 22 (1989).
3. R. Cesareo, A.L. Hanson, G.E. Gigante, L.J. Pedraza, S.Q.G. Mahtaboally, Phys. Rep. **213**, 117 (1992).
4. J.R. Helliwell, Rep. Prog. Phys. **47**, 143 (1984).
5. J.R. Helliwell, *Macromolecular Crystallography with Synchrotron Radiation* (Cambridge University press, Cambridge, 1992).
6. W. Hendrickson, in *Methods in Enzymology*, edited by H. Wyckoff, C. Hirs, N. Timasheff, Vol **15** (Academic Press Inc, Orlando, USA, 1985).
7. J.H. Hubbell, W.J. Veigele, E.A. Briggs, R.T. Brown, D.T. Cromer, R. Jowerton, J. Phys. Chem. Ref. Data **4**, 471 (1975).

8. J.H. Hubbell, I. Øverbø, J. Phys. Chem. Ref. Data **8**, 69 (1979).
9. D. Schaupp, M. Schumacher, F. Smend, P. Rullhusen, J.H. Hubbell, J. Phys. Ref. Data **12**, 467 (1983).
10. L. Kissel, R.H. Pratt, S.C. Roy, Phys. Rev. A **22**, 1970 (1980); L. Kissel, private communication (1996).
11. S.C. Roy, R.H. Pratt, L. Kissel, Rad. Phys. Chem. **41**, 725 (1993), Phys. Rev. A **27**, 285 (1983).
12. L. Kissel, B. Zhou, S.C. Roy, S.K. Sen Gupta, R.H. Pratt, Acta Cryst. A **51**, 271 (1995).
13. K.G. Tirsell, V.W. Silvinsky, P.J. Ebert, Phys. Rev. **12**, 2426 (1975).
14. C. Bui, M. Milazzo, Nuovo Cimento D **11**, 655 (1989).
15. M.L. Garg, R.R. Garg, F. Hennirch, D. Heimurmann, Nucl. Instr. Meth. B **73**, 109 (1993).
16. M. Schumacher, A. Stoffrengen, Z. Phys. A **283**, 15 (1977).
17. P.P. Kane, L. Kissel, R.H. Pratt, S.C. Roy, Phys. Rep. **140**, 75 (1986), Phys. Rev. A **28**, 1509 (1983).
18. D.V. Rao, R. Cesareo, G.E. Gigante, Phys. Scripta **55**, 683 (1997).
19. R.W. James, *The Optical Properties of the Diffraction of the X-rays* (G. Bell and Sons, London, 1948), p. 462.
20. W. Franz, Z. Phys. **98**, 314 (1936).
21. D.T. Cromer, D. Liberman, J. Chem. Phys. **53**, 1891 (1970).
22. L. Kissel, R.H. Pratt, Acta Cryst. A **46**, 170 (1990).
23. D.T. Cromer, D. Liberman, FPRIME code, Los Alamos Scientific Laboratory Report LA-4403 Los Alamos, NM, USA.
24. A.L. Hanson, G.E. Gigante, M. Meron, Phys. Rev. Lett. **61**, 135 (1988).
25. A.L. Hanson, G.E. Gigante, Phys. Rev. A **40**, 171 (1989).
26. D.V. Rao, R. Cesareo, G.E. Gigante, Phys. Scripta **55**, 265 (1997).
27. D.V. Rao, R. Cesareo, G.E. Gigante, Appl. Phys. (Germany) A **64**, 511 (1997).
28. M.J. Berger, J.H. Hubbell, XCOM Photon cross-sections on a personal computer, NBSIR rep. no. **87**-3597, National Bureau of Standards (1987).
29. D.V. Rao, R. Cesareo, G.E. Gigante, X-ray Spectrom. **24**, 175 (1995); Phys. Scripta **53**, 332 (1996).